References and Notes

1. M. W. Denny, *J. Exp. Biol.* **65**, 483 (1976).
2. J. M. Gosline *et al.*, *Endeavour* **10**, 38 (1986).
3. M. Hinman *et al.*, in *Biopolymers* (Springer-Verlag, Berlin-Heidelberg, 1992), pp. 227–254.
4. F. Lucas, *Discovery* **25**, 20 (1964).
5. J. Koover, in *Ecophysiology of Spiders*, W. Nentwig, Ed. (Springer-Verlag, Berlin, Heidelberg, 1987), pp. 160–186.
6. J. Gatesy *et al.*, *Science* **291**, 2603 (2001).
7. F. Vollrath, D. P. Knight, *Nature* **410**, 541 (2001).
8. R. W. Work, *Text. Res. J.* **46**, 485 (1976).
9. J. C. Zemlin, Technical Report No. 69-29-CM (AD684333) (U.S. Army Natick Laboratories, Natick, MA, 1968).
10. D. L. Kaplan *et al.*, in *Silk polymers—Materials Science and Biotechnology*, D. L. Kaplan, W. W. Adams, B. L. Farmer, C. Viney, Eds. (American Chemical Society, Washington, DC, 1994), pp. 2–16.
11. P. A. Guerette, D. G. Ginzinger, B. H. F. Weber, J. M. Gosline, *Science* **272**, 112 (1996).
12. M. Xu, R. V. Lewis, *Proc. Natl. Acad. Sci. U.S.A.* **87**, 7120 (1990).
13. M. B. Hinman, R. V. Lewis, *J. Biol. Chem.* **267**, 19320 (1992).
14. M. B. Hinman, J. A. Jones, R. V. Lewis, *Trends Biotechnol.* **18**, 374 (2000).
15. C. Y. Hayashi, N. H. Shipley, R. V. Lewis, *Int. J. Biol. Macromol.* **24**, 271 (1999).
16. J. M. Gosline, P. A. Guerette, C. S. Ortlepp, K. N. Savage, *J. Exp. Biol.* **202**, 3295 (1999).
17. C. Y. Hayashi, R. V. Lewis, *Science* **287**, 1477 (2000).
18. S. R. Fahnestock, S. L. Irwin, *Appl. Microbiol. Biotechnol.* **47**, 23 (1997).
19. J. T. Prince, K. P. McGrath, C. M. DiGirolamo, D. L. Kaplan, *Biochemistry* **34**, 10879 (1995).
20. S. R. Fahnestock, L. A. Bedzyk, *Appl. Microbiol. Biotechnol.* **47**, 33 (1997).
21. R. V. Lewis, M. Hinman, S. Kothakota, M. J. Fournier, *Protein. Expr. Purif.* **7**, 400 (1996).
22. S. Arcidiacono, C. Mello, D. Kaplan, S. Cheley, H. Bayley, *Appl. Microbiol. Biotechnol.* **49**, 31 (1998).
23. S. R. Fahnestock, Z. Yao, L. A. Bedzyk, *Rev. Mol. Biotechnol.* **74**, 105 (2000).
24. J. Scheller, K.-H. Guhrs, F. Grosse, U. Conrad, *Nature Biotechnol.* **19**, 573 (2001).
25. R. L. Lock, U.S. Patent 5,252,285 (1993).
26. O. Liivak *et al.*, *Macromolecules* **31**, 2947 (1998).
27. K. A. Trabbic, P. Yager, *Macromolecules* **31**, 462 (1998).
28. A. Seidel *et al.*, *Macromolecules* **31**, 6733 (1998).
29. A. Seidel *et al.*, *Macromolecules* **33**, 775 (2000).
30. S. R. Fahnestock, International Patent Application, Publication No. WO 94/29450 (1994).
31. J. P. O'Brien *et al.*, *Adv. Mater.* **10**, 1185 (1998).
32. Complete experimental protocols and figures are available on *Science* Online at www.sciencemag.org/cgi/content/full/295/5554/472/DC1.
33. G. C. Candelas, C. Arroyo, C. Carrasco, R. Dompenciel, *Dev. Biol.* **140**, 215 (1990).
34. P. M. Lizardi, V. Mahdavi, D. Shields, G. C. Candelas, *Proc. Natl. Acad. Sci. U.S.A.* **76**, 6211 (1979).
35. Fiber spinning. Recombinant–spider silk fibers were wet spun into a coagulation bath containing methanol and water. A 5-μl sample of spin solution (10 to 28%) was injected into a small volume of methanol at various concentrations. The ability of the spin solution to coagulate, as well as the speed of coagulation, was considered in choosing the appropriate methanol concentration. The "prototype spinning apparatus" for rc–spider silk fiber production was a Harvard Apparatus Infusion/Withdrawal Pump (Harvard Instruments, Natick, MA) equipped with a specialized microspinner (cavity volume 0.5 ml, 5 mm internal diameter), and a 6-cm-long, 0.005-inch (0.125 mm internal diameter) PEEK HPLC tubing (Sigma-Aldrich) was used as a spinneret. As little as 25 μl of dope rc–spider silk solution could be spun. Spin solutions were extruded into the coagulation bath at a pump speed of 2 to 10 μl/min. Single-drawn fibers were hand-drawn while in the methanol/water coagulation bath. Double-drawn fibers were drawn first in the bath as described above, followed by drawing in water at ambient temperature. The fiber was held constrained at both ends while being moved to the water bath as well as while being air-dried.
36. R. W. Work, *Text. Res. J.* **47**, 650 (1977).
37. C. Viney, in *Structural Biological Materials: Design and Structure-Property Relationships*, M. Elices, Ed. (American Chemical Society, Washington, DC, 2000), vol. 10, pp. 295–333.
38. Y. Termonia, in *Structural Biological Materials: Design and Structure-Property Relationships*, M. Elices, Ed. (American Chemical Society, Washington, DC, 2000), vol. 10, pp. 271–291.
39. C. Viney *et al.*, in *Silk Polymers—Materials Science and Biotechnology*, D. L. Kaplan, W. W. Adams, B. L. Farmer, C. Viney, Eds. (American Chemical Society, Washington, DC, 1994), pp. 120–136.
40. Y. Termonia, in *Structural Biological Materials: Design and Structure-Property Relationships*, M. Elices, Ed. (American Chemical Society, Washington, DC, 2000), vol. 10, pp. 337–349.

41. We thank R. Lewis and J. M Gosline for providing cDNAs, and S. Islam for critical evaluation of the fiber mechanical testing data; J. Turner for valuable discussions; R. Keyston for help during the early stages of this work; and members of our laboratory for their support. We also thank D. Ziegler (Natick Soldier Center) for the SEM micrographs and S. Fossey, C. Mello, R. Segars, and J. Herbert (Natick Soldier Center) for valuable discussions. This work was supported by the Defense Industry Research program of the Canadian Department of Natural Defense (Val Cartier, PQ).

28 August 2001; accepted 11 December 2001

Positive Mass Balance of the Ross Ice Streams, West Antarctica

Ian Joughin[1]* and Slawek Tulaczyk[2]*

We have used ice-flow velocity measurements from synthetic aperture radar to reassess the mass balance of the Ross Ice Streams, West Antarctica. We find strong evidence for ice-sheet growth (+26.8 gigatons per year), in contrast to earlier estimates indicating a mass deficit (−20.9 gigatons per year). Average thickening is equal to ~25% of the accumulation rate, with most of this growth occurring on Ice Stream C. Whillans Ice Stream, which was thought to have a significantly negative mass balance, is close to balance, reflecting its continuing slowdown. The overall positive mass balance may signal an end to the Holocene retreat of these ice streams.

Over the past several decades there has been concern that the marine-based West Antarctic Ice Sheet might collapse within the next several centuries, raising sea level by 5 to 6 m (*1*). Underlain by a thick layer of marine sediments, this ice sheet has exhibited considerable change in flow over the last millennium, particularly along the Siple Coast in the Ross Sea Sector (*2*), and since the last glacial maximum, the grounding line (the point where the ice sheet loses contact with its bed and begins to float) has retreated nearly 1300 km along the western side of the Ross Embayment. The chronology established for this retreat suggests mean grounding-line migration rates of 120 m/year (*3*). Although other processes might intervene, extrapolation of these rates has been used to predict a 4000-year lifetime for the West Antarctic Ice Sheet (*4*). Although this is a much longer period than earlier estimates (*5*) that predict a collapse over a few centuries, it does imply a sea-level rise of 12.5 to 15 cm per century.

Hypotheses of continued grounding-line retreat and possible collapse have been supported by an estimate of −20.9 ± 13.7 Gton/year (*6*, *7*) for the mass balance of the Ross Ice Streams (A to F) (Fig. 1). This negative value by Shabtaie and Bentley (S&B) (*6*) implies that ice discharge (loss) exceeds accumulation by ~25%, causing the ice sheet to thin and the grounding line to retreat. Much of this imbalance has been attributed to Whillans Ice Stream (formerly known as Ice Stream B), but negative imbalances were also found for the other Ross Ice Streams, with the exception of Ice Stream C, which stagnated 150 years ago (*8*). More recent analyses (*9*) based on similar data have estimated comparable negative imbalances on Whillans Ice Stream.

The ice-discharge estimates in earlier studies relied on relatively sparse in situ measurements of ice-flow velocity (*10*). For some ice streams, the S&B discharge estimates were based on only one or two velocity measurements (*6*). We used spatially dense estimates of ice-flow velocity (Fig. 1) afforded by Interferometric Synthetic Aperture Radar

[1]Jet Propulsion Laboratory, California Institute of Technology, Mailstop 300-235, 4800 Oak Grove Drive, Pasadena, CA 91109, USA. [2]Department of Earth Sciences, A208 Earth and Marine Sciences Building, University of California, Santa Cruz, Santa Cruz, CA 95064, USA.

*E-mail: ian@radar-sci.jpl.nasa.gov, tulaczyk@es.ucsc.edu

(InSAR) (*11*) to reassess the mass balance of the Ross Ice Streams.

We began by determining the catchments for individual ice streams (*12*). As in earlier studies, we then estimated the ice-discharge flux through a "gate" located near the grounding line at the downstream end of each catchment (*13*). The total accumulation for each catchment area above its respective gate was determined by integrating gridded accumulation data (*14*). The difference between the accumulation (input) and discharge (output) gives the mass balance for the catchment. The results with uncertainties are tabulated in Table 1.

Our results indicate that, contrary to earlier estimates, the mass balance of this sector of the West Antarctic Ice Sheet is positive (26.8 ± 14.9 Gton/year). Ice Streams D and E and the combined outflow of Ice Stream A and Whillans Ice Stream are in balance to within the 2σ limits of the uncertainty. This is consistent with radar altimetry observations that show little thickening or thinning over the catchments of Ice Streams D and E (*15*). Ice stream F is significantly positive, but its contribution to the overall total is small relative to that of the other ice streams. Stagnant Ice Stream C has a strongly positive mass balance because of its negligible outflow, and it is the major contributor to the overall positive mass balance for the region. Thus, the positive imbalance is driven not by climate-related changes in accumulation or melt, but rather by the internal ice-stream dynamics that led to the stoppage of Ice Stream C.

There is a 47.7 Gton/year difference in our estimate of net balance (+26.8 Gton/year) compared with the S&B estimate (−20.9 Gton/year) (*6*). The largest component of this difference is a change in estimated discharge fluxes (27.1 Gton/year). A breakdown of the discharge-flux differences is given in Table 2. Several studies have documented a deceleration on Ice Stream A and Whillans Ice Stream (*9*) with the most current estimate yielding an average deceleration rate of 5.0 m/year^2 from 1974 to 1997 (*16*). As indicated in Table 2, the 23% deceleration over this period accounts for 10.6 Gton/year (38%) of the total differ-

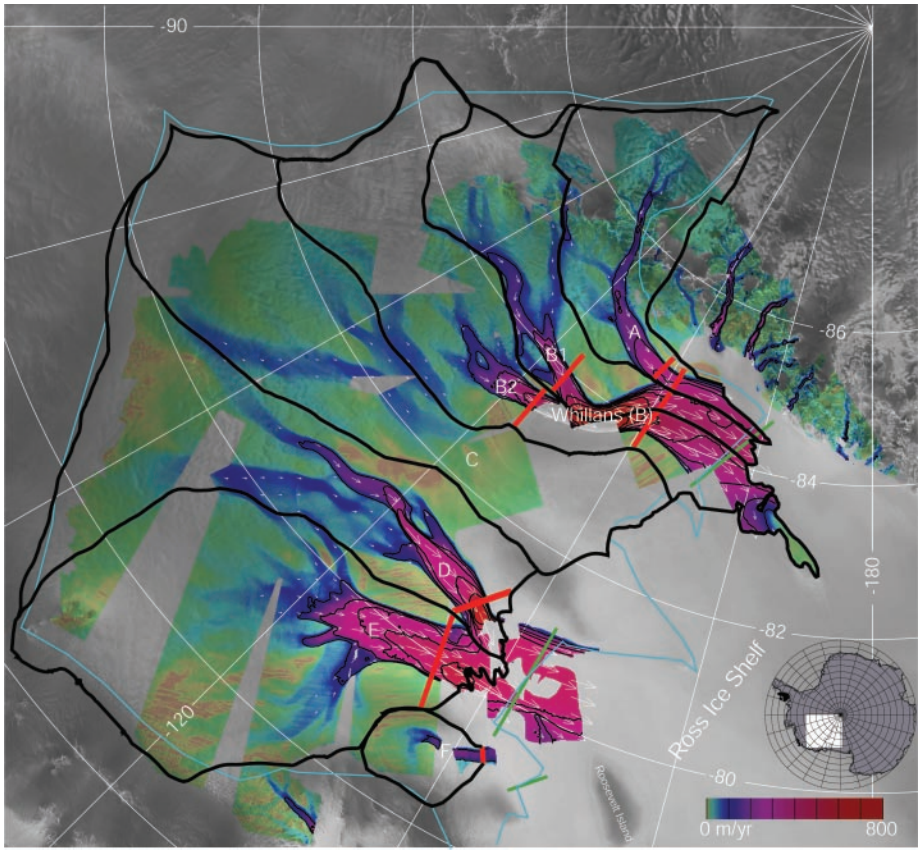

Fig. 1. Ice-flow velocity (colors) over radar imagery from the RADARSAT Antarctic Mapping Project Mosaic (*41*). Flow velocity at 100 m/year intervals is contoured with thin black lines. White vectors show subsampled velocity vectors in fast-moving areas. Catchment boundaries (*12*) for individual ice streams are plotted with thick black lines. Flux gates used in discharge calculations are shown with red lines. Green lines show the locations of the S&B flux gates (*6*), and the light blue line shows the outline of the S&B catchment. The white box on the inset map shows the location of the study area.

Table 1. Discharge and accumulation fluxes for the Ross Ice Streams. The summed total excludes the first three entries because the combined flux through these gates is included by the wider gate farther downstream (see Fig. 1). All accumulation numbers for individual ice streams are based on the average of two accumulation maps (*14*), except where noted. The last row shows the S&B results for their catchment shown in Fig. 1.

Gate	Accumulation above gate (10^{12} kg year^{-1})	Discharge flux (10^{12} kg year^{-1})	Difference (10^{12} kg year^{-1})	Area above gate (km^2)	Average accumulation rate (kg m^{-2} year^{-1})
Ice Stream A	10.1 (1.5)	8.0 (0.3)	2.10 (1.5)	72,400	139
Whillans B1	8.0 (1.2)	12.7 (0.4)	−4.70 (1.3)	52,400	153
Whillans B2	12.9 (1.9)	10.3 (0.4)	2.60 (2.0)	87,900	146
Ice Stream A and Whillans Ice Stream	32.8 (4.9)	30.3 (0.7)	2.50 (5.0)	235,200	139
Ice Stream C	20.5 (3.1)	0.5 (0.2)*	20.1 (3.1)	153,400	134
Ice Stream D	19.0 (2.9)	15.3 (0.4)	3.75 (2.9)	140,300	136
Ice Stream E	23.5 (3.5)	24.4 (0.7)	−0.85 (3.6)	175,200	134
Ice Stream F	2.8 (0.4)	1.5 (0.1)	1.35 (0.4)	16,800	171
Total AW+C+D+E+F	98.8 (14.8)	72.0 (1.1)	26.8 (14.9)	721,000	137
	102.9 (15.4)†		30.8 (15.4)†		142†
	94.7 (14.2)‡		22.7 (14.2)‡		131‡
Shabtaie and Bentley (1987)§	83.4 (12.8)§	110.6 (4.6)§	−20.9 (13.7)§‖	701,000§	119§

*Ice Stream C discharge is from Shabtaie and Bentley (*6*). †Using the Giovinetto and Zwally accumulation map (*36*). ‡Using Vaughan *et al.* accumulation map (*37*). §Over the S&B catchment area shown in Fig. 1. ‖Includes additional mass loss (3.5 Gton/year) due to basal melt.

ence in discharge. For Ice Streams D to F, there is little evidence of temporal variation in velocity over this period. The differences in discharge estimates for these ice streams are attributable to a variety sources, as shown in Table 2.

An additional difference of 3.5 Gton/year can be accounted for by the inclusion of basal melt beneath the grounded ice in the S&B estimate. We believe basal melt to be about an order of magnitude smaller than this amount and exclude it from our calculations (*17*).

As illustrated in Fig. 1, the overall catchment boundary we have derived differs from that used by Shabtaie and Bentley, making comparison of our basinwide accumulation estimate with the S&B estimate difficult. We performed a detailed comparison of accumulation over the S&B catchment area that leads us to conclude that the S&B results underestimate accumulation (*18*). This accounts for most of the revision in mass balance that is attributable to differences in accumulation. A much smaller contribution to this revision is attributable to our use of the average of two accumulation maps.

Although Whillans Ice Stream is nearly in balance at present, it was clearly out of balance in the past, as indicated by the roughly 23% decrease in velocity from 1974 to 1997 (*16*). It is unclear how long the deceleration has been underway, but it is likely that the discharge could have been greater still before 1974 (*16*). Although deceleration of Whillans Ice Stream has helped to restore its mass balance, changes in the ice surface geometry and resulting drainage patterns have also contributed. The surface of Whillans B2 (Whillans Branch 2) is substantially lower than that of Ice Stream C. This difference can be attributed, in part, to a thickening on Ice Stream C since stagnation (*19*) and a thinning of Whillans B2 (*9*), which is consistent with a past negative mass balance. As indicated in earlier work (*19*) and to greater extent by the catchments shown in Fig. 1, the drainage for Whillans B2 has expanded to include some of the area that formerly fed Ice Stream C. Furthermore, on the southern side of the B2 catchment, the boundary extends to the edge of a tributary feeding Whillans B1 (Whillans Branch 1), suggesting capture of part of its catchment by Whillans B2. This potential "ice piracy" may explain the negative mass balance for Whillans B1 and what is likely a relatively recent shift to a positive mass balance on Whillans B2. Our results represent an average over the catchment and, thus, are not inconsistent with estimates of local thinning on Whillans Ice Stream (*9*).

Critical to prediction of how this sector of the ice sheet will evolve over the next few centuries is an understanding of the future behavior of Ice Stream A and Whillans Ice Stream. These ice streams are currently in balance so that the observed deceleration could indicate that the ice sheet is responding as needed to compensate for a past imbalance. Field measurements collected in 1998 suggest that the deceleration may be continuing unabated (*20*). If so, then any restoration of balance is likely to "overshoot" and yield at least a temporary shift to a positive mass balance. Such a shift might be well within the degree of ice-flow variability that has been inferred for the region over the last 1000 years (*2*).

The deceleration could also indicate more than a simple restoration of mass balance. Thermodynamic models of ice-stream evolution show that ice streams may be inherently cyclic in their behavior, with switches between active ("purge") and inactive ("binge") phases occurring with a periodicity of several thousand years (*21*, *22*). If deceleration on the ice plain fed by Ice Stream A and Whillans Ice Stream continues at its current rate, then outflow will cease in 70 to 80 years. Thus, these ice streams may be undergoing a transition from the purge to the binge phase, as seems to have occurred on neighboring Ice Stream C about 150 years ago (*8*). Modeling of ice-stream behavior indicates that ice-stream stoppages may be triggered by a prolonged period of negative mass balance, which leads to ice-stream thinning that, in turn, switches the basal thermal regime from melting to freezing (*21*, *22*). Freezing removes water from the subglacial zone, thereby increasing basal resistance and decreasing ice-stream velocity. Through nonlinear positive feedback between basal freezing and shear heating, freeze-on-driven ice-stream slowdown may be a runaway process that, once initiated, leads to complete ice-stream shutdown (*23*). A paucity of direct constraints on the rates of sub–ice stream meltwater production and redistribution (*24*, *25*) makes it difficult to rule out the possibility that the observed slowdown of Whillans Ice Stream is just a decadal-scale fluctuation. The recent stoppage of Ice Stream C (*8*), however, coupled with the results of thermodynamic ice-stream models, makes it plausible that the current slowdown of Whillans Ice Stream could continue to a complete stagnation. This would decrease outflow by 30.3 Gton/year, reduce collective discharge to 42% of accumulation, and yield an average thickening rate of 8.3 cm/year over the total catchment area shown in Fig. 1.

Even with a complete shutdown of Ice Stream A and Whillans Ice Stream, the direct impact on sea level is not large. If this stagnation were to occur, a positive imbalance of 57 Gton/year would lower sea level by 0.16 mm/year compared to a rise of 0.06 mm/year with the S&B estimate (*6*). For comparison, this positive imbalance would be nearly equivalent to completely blocking the flow of the Missouri River (72 Gton/year at U.S. Geological Service gage in Hermann, Missouri). Of more importance, our results, although providing

Table 2. Comparison of InSAR discharge estimates (see Table 1) with S&B estimates (*6*). Most of the difference in discharge for Ice Stream A and Whillans Ice Stream can be attributed to velocity change and accumulation between gates. Much of the remaining difference may be the result of measurement error and additional flow from glaciers that discharge to the ice shelf near the southern end of the S&B gate (see Fig. 1). We estimate with a large uncertainty that the S&B gate for Ice Streams D and E was too wide by 17% and contains a substantial amount of slow-moving ice. Accounting for this difference and accumulation between gates yields a remaining difference with opposite sign. This negative difference is likely the result of some combination of remaining uncertainty in the S&B gate width, diversion of flow between gates (e.g., toward the S&B F gate), and basal melting on the floating part of the shelf (*40*). The difference at the S&B Ice Stream F gate is largely attributable to flux from Ice Streams D and E that passes through this gate.

Gate	InSAR discharge flux (10^{12} kg year^{-1})	S&B discharge flux (10^{12} kg year^{-1})	Difference S&B − Insar (10^{12} kg year^{-1})	Quantifiable difference (10^{12} kg year^{-1})	Remaining difference (10^{12} kg year^{-1})
Ice Stream A and Whillans Ice Stream	30.3 (0.7)	46.0 (2.4)	15.7 (2.5)	12.3 = 10.6* + 1.7†	3.4
Ice Stream C	0.5 (0.2)	0.5 (0.2)	0 (0.2)	0	0
Ice Stream DE	39.7 (0.8)	44.3 (2.8)	4.6 (2.9)	10.1 = 7.5‡ + 2.6†	−5.5
Ice Stream F	1.5 (0.4)	8.3 (1.3)	6.8 (1.4)	6.8§	0
Total	72 (1.1)	99.1 (3.9)	27.1 (4.1)	29.2	−2.1

*Decrease due to 23% decline in interval between velocity measurements (*16*). †Accumulation between gates. ‡Gate width in Shabtaie and Bentley (*6*) is ~17% too wide. §Flux from D/E attributed to Ice Stream F (see Fig. 1).

only a limited "snapshot of mass balance," suggest a reduced probability for scenarios that involve continued inland migration of the grounding line, a near-term catastrophic collapse, and a substantial rise in sea level. This analysis covers only the Ross Sea sector of the ice sheet, and negative imbalances are observed in other areas of West Antarctica such as Pine Island and Thwaites Glaciers (*26*).

A reduction in discharge could have important implications for the near-term stability of the Ross Ice Shelf, which exists largely as a result of high discharge by ice streams into the Ross Embayment. The combined stagnation of Whillans Ice Stream and Ice Streams A and C would reduce discharge across the grounding line of the Ross Ice Shelf by roughly 25% from that before the shutdown of Ice Stream C. Such a reduction in discharge could cause the ice shelf to thin and could trigger a retreat and/or break-up. Additional impetus for retreat/break-up may come from future climatic warming that appears to have helped to destabilize some smaller ice shelves along the Antarctic Peninsula (*27*). Over time scales on the order of decades to centuries, ice shelves may represent the most vulnerable element of the West Antarctic ice sheet/shelf system. Break-up of the Ross Ice Shelf alone would expose ~400,000 km^2 of new shallow sea surface area and could have important implications for exchange of energy and water between the ocean and the atmosphere/ice-sheet system in the region. Moreover, brine exclusion during sea-ice formation could turn this newly exposed polar continental shelf into a key source of bottom ocean water. This strengthened Antarctic bottom-water formation could outcompete the North Atlantic source of bottom water and switch the global ocean into a new mode of thermohaline circulation, with global climatic implications (*28*).

The positive imbalance we observe and the trend toward a potentially larger imbalance are evocative of an ice sheet in advance rather than in retreat. There is ample evidence for a large retreat of the West Antarctic ice sheet over the last several thousand years (*3*, *4*). The observed positive imbalance developed within just the last two centuries as a result of the stoppage of Ice Stream C and slowdown of Whillans Ice Stream. If the current positive imbalance is not merely a part of decadal- or century-scale fluctuations, it represents a reversal of the long-term Holocene retreat.

References and Notes

1. R. B. Alley, R. A. Bindschadler, *Antarctic Res. Ser.* **77** (American Geophysical Union, Washington, DC, 2001).
2. M. A. Fahnestock, T. A. Scambos, R. A. Bindschadler, G. Kvaran, *J. Glaciol.* **46**, 155 (2000).
3. H. Conway, B. L. Hall, G. H. Denton, A. M. Gades, E. D. Waddington, *Science* **286**, 5438 (1999).
4. R. Bindschadler, *Science* **282,** 5388 (1998).
5. J. H. Mercer, *Int. Assoc. Hydrol. Sci. Publ. 179* (1968).
6. S. Shabtaie, C. R. Bentley, *J. Geophys. Res.* **92**, 2 (1987).
7. Accumulation values in Shabtaie and Bentley (*6*) were expressed in ice-equivalent volume. We have rescaled these values to mass equivalent using 910 kg/m^3 for the density of ice.
8. R. Retzlaff, C. R. Bentley, *J. Glaciol.* **39**, 133 (1993).
9. I. M. Whillans, C. R. Bentley, C. J. van der Veen, *Antarctic Res. Ser.* **77** (American Geophysical Union, Washington, DC, 2001).
10. R. H. Thomas, D. R. MacAyeal, D. H. Eilers, D. R. Gaylord, *Antarctic Res. Series* **42** (American Geophysical Union, Washington, DC, 1984).
11. Interferometric phase data were used to obtain velocities where the phase data could be unwrapped (e.g., <125 m/year). Where crossing swaths were available, both horizontal vector components were derived from the phase data (*29*). In regions with only single-track coverage, speckle tracking was used for the along-track component. Speckle tracking was used for both components where displacements were too large to allow phase unwrapping. Gaps in coverage on the lower parts of Ice Streams D, E, and F were filled by feature-tracking data from optical imagery (*30*). Several hundred ground-based velocity measurements were used to solve for the interferometric baseline parameters. The residual difference between control points and estimated velocity is >5 m/year and is indicative of the random component of the velocity error (*16*, *31*). Systematic errors may be higher in areas not well constrained by the control velocities.
12. Catchments boundaries were derived by using a combination of velocity and elevation data. Where velocities were sufficiently large to avoid ambiguity in flow direction, we used velocity-derived flow lines to determine boundaries. In other areas we used slope-derived flow lines with either the RADARSAT Antarctic Mapping Mission DEM (*32*) or higher resolution airborne observations of elevation where available (*33*).
13. For Whillans Ice Stream and Ice Streams A, D, and E, we used profiles of ice thickness from airborne radar echo sounding (*30*, *34*). For Ice Stream F, we relied on a gridded map of ice thickness (*35*). Gridded data were also used to extend the lengths of a few profiles to the catchment-divide edges. We corrected the ice-thickness values by subtracting 12 m to account for the reduced density of firn (*30*). Fluxes were computed as the integral of the product of thickness and the component of velocity normal to the gate. Errors were determined assuming 5 m/year (*16*) velocity and 10-m (*6*) thickness errors.
14. We estimated integrated accumulation using the average of two accumulation maps (*36*, *37*) that were based on essentially the same source data. The accumulation totals for the two maps differ by ~10%, which is indicative of the variability introduced by regridding. Both maps have their own merits, and it is difficult to tell which is more accurate. As a result, unless otherwise noted, all accumulation values are based on the average of the two maps. We use a value of 15% for the error in the catchment-wide accumulation totals, which reflects the combination of accumulation map error and catchment area error and is consistent with errors derived for other studies (*6*, *9*).
15. D. J. Wingham, A. J. Ridout, R. Scharroo, R. J. Arthern, C. K. Shum, *Science* **291**, 5388 (1998).
16. I. R. Joughin, S. Tulaczyk, R. Bindschadler, S. Price, in preparation.
17. Force-balance estimates indicate that lateral shear can provide much of the resistance to driving stress where the bed is weak (*9*). With lower estimates of resistance at the bed, basal-melt estimates are much smaller (*16*, *23*, *38*) than for the S&B estimate (*6*).
18. Of the two accumulation maps we used, the one by Giovinetto and Zwally (*36*) has undergone only minor revision from the map used by Shabtaie and Bentley (*6*), so there should be no appreciable differences in accumulation. The S&B basinwide average accumulation rate (119 kg m^{-2} year^{-1}) is much smaller, however, than the value (142 kg m^{-2} year^{-1}) we obtained using the Giovinetto and Zwally (*36*) map. Similar differences occur when comparing the S&B accumulation rates with those obtained by other authors using the same map (*36*, *37*, *39*). One explanation for this discrepancy is that the S&B values were scaled incorrectly when they were converted from water to ice equivalent. If such an error (scaling by 0.91 instead of 1/0.91) is accounted for, then the S&B accumulation rates fall into agreement with other estimates. We estimated the area of the S&B catchment region (Fig. 1) as 797,000 km^2 compared with their estimate of 701,000 km^2. The difference is too large to be explained by the error we incurred in digitizing their basin boundary. An earlier study by Giovinetto and Bentley (*39*) contained errors in basin area because they did not account for latitude dependence when they corrected the area distortion introduced by the polar stereographic projection (*37*). If we assume that an error of the same magnitude occurred in the S&B data, then their estimate can be rescaled to 783,000 km^2, which agrees with our estimate to within the digitization error. If we assume errors in both area and accumulation rate, then the S&B estimate of accumulation can be revised from 83.4 Gton/year to 112.3 Gton/year, which agrees well with our estimate of 110.6 Gton/year for the S&B catchment.
19. S. F. Price, R. A. Bindschadler, C. L. Hulbe, I. Joughin, *J. Glaciol.*, **47**, 157 (2001).
20. R. Bindschadler, unpublished data. Field measurements of velocity were collected at several sites 15 months after the collection of the RADARSAT data. For a deceleration rate of 5 m/year^2, this would yield a velocity change of 6.25 m/year. Several points suggest continued deceleration. Because the nominal velocity error for the InSAR data is 5 m/year, any suggestion of continued deceleration is near the detection threshold.
21. D. R. MacAyeal, *Paleoceanography* **8**, 775 (1993).
22. A. J. Payne, P. W. Dongelmans, *J. Geophys. Res. Solid Earth* **102**, B6 (1997).
23. S. Tulaczyk, B. Kamb, H. F. Engelhardt, *J. Geophys. Res.* **105**, 1 (2000).
24. H. Engelhardt, B. Kamb, *J.Glaciol.* **43**, 207 (1997).
25. S. Anandakrishnan, R.B. Alley, *Geophys. Res. Lett.* **24**, 3 (1997).
26. E. Rignot, D. G. Vaughan, M. Schmeltz, T. Dupont, D. R. MacAyeal, *Ann. Glaciol.*, in press.
27. D. G. Vaughan, C. S. M. Doake, *Nature* **379**, 6563 (1996).
28. G. H. Denton, *J. Quat. Sci.* **15,** 4 (2000).
29. I. Joughin, R. Kwok, M. Fahnestock, *IEEE Trans. Geosci. Remote Sens.* **36**, 25 (1998).
30. R. Bindschadler, P. Vornberger, D. Blankenship, T. Scambos, R. Jacobel, *J. Glaciol.* **43**, 142 (1996).
31. I. Joughin *et al.*, *Science*, **286**, 5438 (1999).
32. H. Liu, K. Jezek, B. Li, *J. Geophys. Res.* **104**, 10 (1999).
33. D. D. Blankenship *et al.*, *Am. Geophys. U. Antarctic Res. Ser.* **77**, 105 (2001).
34. R. Retzlaff, N. Lord, C. R. Bentley, *J. Glaciol.* **39**, 133 (1993).
35. M. B. Lythe, D. G. Vaughan, *J. Geophys. Res.* **106**, 6 (2001).
36. M. Giovinetto, J. Zwally, *Ann. Glaciol.* **31**, 171 (2000).
37. D. G. Vaughan, J. L. Bamber, M. Giovinetto, J. Russell, A. P. R. Cooper, *J. Climate* **12,** 933 (1999).
38. C. F. Raymond, *J. Glaciol.* **46**, 155 (2000).
39. M. Giovinetto, C. R. Bentley, *Antarct. J. U.S.* **20,** D4 (1985).
40. D. R. MacAyeal, R. H. Thomas, *J. Glaciol.* **32**, 72 (1986).
41. K. C. Jezek, *Ann. Glaciol.* **29**, 286 (1999).

42. We thank M. Giovinetto and D. Vaughan for copies of their accumulation maps and for comments on the manuscript. We also acknowledge the Alaska Synthetic Aperture Radar (SAR) facility (University of Alaska) for the raw SAR data needed for the

velocity measurements and C. R. Bentley and R. Bindschadler for ice-thickness profile data. K. Jezek provided the RADARSAT image mosaic. The RAMP DEM and the ground-based and LandSAT feature–tracked measurements of velocity were provided by the National Snow and Ice Data Center. Comments by T. Scambos and C. R. Bentley improved the revised manuscript. I.J. performed this work at the Jet Propulsion Laboratory, California Institute of Technology, under contract with the National Aeronautics and Space Administration. S.T was funded by NSF–Office of Polar Program grants 9873593 and 0096302.

5 October 2001; accepted 14 December 2001

Experimental Detection of Tetranitrogen

F. Cacace,* G. de Petris, A. Troiani

Tetranitrogen (N_4), which has been the subject of great theoretical interest, has been prepared from the N_4^+ cation and positively detected as a gaseous metastable molecule with a lifetime exceeding 1 microsecond in experiments based on neutralization-reionization mass spectrometry. An examination of the geometry of N_4^+ and the fragmentation pattern of the $^{14}N_2{}^{15}N_2$ neutral molecule has revealed that the latter is characterized by an open-chain geometry with two distinct, closely bound N_2 units joined by a longer weaker bond.

During the last decade, the neutral N_4 molecule has been the subject of intense and sustained theoretical scrutiny, aimed at evaluating the structure, stability, and properties of this experimentally unknown species (*1*–*13*). Apart from the molecule's fundamental significance, such unusual interest is motivated by the potential of N_4 as a "pure" high-energy density material. Theory predicts that, whereas certain N_4 isomers, such as tetraazatetrahedrane, are metastable and long lived, their dissociation into two environmentally benign N_2 molecules is very exothermic, releasing about 800 kJ mol^{-1} (*7*, *10*–*12*).

Despite the considerable help provided by the theoretical identification and characterization of the target species, preparing and detecting N_4 has posed a formidable challenge to experimentalists. None of the suggested routes, involving the combination of a nitrogen atom with an $N_3^{\cdot}$ radical, binding of two excited N_2 ($A^3\Sigma_u^+$) molecules, and N_4 extrusion from larger, polycyclic molecules, proved viable (*14*).

Here, we report the preparation, positive detection, and characterization as a long-lived gaseous species of an N_4 molecule obtained by a different approach—the one-electron reduction of the gaseous N_4^+ cation by neutralization-reionization (NR)–mass spectrometry (*15*–*17*). We have used this technique effectively for the preparation and detection of other elusive species, including HO_3 (*18*), the [H_2O^+ O_2^-] charge-transfer complex (*19*), and O_4 (*20*).

The charged precursor chosen, N_4^+, is long known and thoroughly characterized as a result of mass spectrometric (*21*, *22*), matrix isolation (*23*, *24*), spectroscopic (*25*, *26*), and theoretical studies (*23*, *27*–*31*), motivated by its role in N_2 plasmas and in stratospheric chemistry. Ground-state and excited N_4^+ ions are conveniently obtained by electron bombardment of N_2 (*32*). Our experimental approach was as follows. The N_4^+ ions formed in the chemical ionization (CI) source of a multisector mass spectrometer of EBE-TOF configuration (where E stands for electrostatic, B for magnetic sectors, and TOF for an orthogonal time-of-flight analyzer) were accelerated to 4 to 8 kV and mass selected. The N_4^+ ions underwent two consecutive collision events in the two separate cells located along the beam path, each containing a suitable target gas. In the first cell, a fraction of the ions was neutralized by electron transfer from the molecules of the first target gas, A, yielding N_4

$$N_4^+ \xrightarrow[-A^+]{+A} N_4 \qquad (1)$$

together with neutral and charged fragments. The parent ions surviving neutralization and any charged fragments were removed by a high-voltage deflecting electrode, so that only a fast beam of neutral species entered the second cell, where reionization occurred upon collision with the molecules of the second targed gas, B, giving cations.

$$N_4 \xrightarrow[-e]{+B} N_4^+ \qquad (2)$$

Detection of a "recovery" peak, that is of a charged species with the same mass-to-charge (m/z) ratio as the original N_4^+ ions, in the NR spectra (Fig. 1A) of $^{14}N_4^+$, $^{14}N_2{}^{15}N_2^+$, and $^{15}N_4^+$ ions at m/z = 56, 58, and 60, respectively, positively demonstrates the occurrence of the reaction sequence in equations 1 and 2 and hence the existence of a neutral N_4 species with a lifetime in excess of the flight time from the neutralization to the reionization cell, i.e, ~1 μs.

Structural insight is provided by the isotopic composition of the N_2^+ fragments displayed by the NR spectra that can originate only from the uncharged species formed in the neutralization and/or in the reionization process. As expected, $^{14}N_4$ gives only $^{14}N_2^+$, and $^{15}N_4$ gives only $^{15}N_2^+$, but $^{14}N_2{}^{15}N_2$ gives equal amounts of $^{14}N_2^+$ and $^{15}N_2^+$, without detectable formation of the isotopically mixed $^{14}N^{15}N^+$ fragment. This pattern strongly suggests that the N_4 molecule contains two distinct N_2 units that maintain their identity without exchanging their constituent atoms and that the four N atoms of N_4 are inequivalent.

As to the structure of the N_4 species detected, and its identification with one of the theoretically predicted isomers, useful criteria are provided by the intrinsic features of NR spectrometry. Detection of a neutral species can occur only if its dissociation requires overcoming a sizeable barrier, on the order of 40 kJ mol^{-1} (*15*–*17*), and the vertical character of the neutralization process allows survival of the neutral molecule only if its geometry is not significantly different from that of the parent ion (the transition displays adequate Franck-Condon factors).

In view of the latter requirement, the connectivity of the N_4^+ ions used in the NR experiments has been probed by collisionally activated dissociation (CAD)–mass spectrometry and the assignment of the polyatomic fragments confirmed by examining their further dissociation according to the technique known as tandem mass spectrometry (MS/MS). The CAD spectrum of $^{14}N_4^+$ (Fig. 1B) displays the $^{14}N^+$, $^{14}N_2^+$, and $^{14}N_3^+$ fragments; and the CAD spectrum of $^{15}N_4^+$ displays the $^{15}N^+$, $^{15}N_2^+$, and $^{15}N_3^+$ fragments. The CAD spectrum of the $^{14}N_2{}^{15}N_2^+$ ion displays $^{14}N^+$ and $^{15}N^+$, $^{14}N_2^+$ and $^{15}N_2^+$, and $^{14}N_2{}^{15}N^+$ and $^{14}N^{15}N_2^+$ fragments. The nature and relative abundances of the fragments are consistent with the connectivity assigned to N_4^+ in its $^2\Sigma_m^+$ ground state by experimental and theoretical studies (*21*–*31*), whose results characterize the cation as an open-chain species with two closely bound N_2 units joined by a longer, weaker bond. Based on the observed formation of the N_3^+ ion in the CI source, and as a fragment in the CAD spectra of N_4^+, it cannot be excluded that excited species, in particular the $N_4^+(^4A')$ in the first-quartet state, are present in the N_4^+ population.

Dipartimento di Studi di Chimica e Tecnologia delle Sostanze Biologicamente Attive, Università di Roma "La Sapienza," Piazzale Aldo Moro, 5–00185 Roma, Italy.

*To whom correspondence should be addressed. E-mail: fulvio.cacace@uniroma1.it

Positive Mass Balance of the Ross Ice Streams, West Antarctica

Ian Joughin and Slawek Tulaczyk

Science **295** (5554), 476-480.
DOI: 10.1126/science.1066875